IEEE Photonics Journal
An IEEE Photonics Society Publication

Open Access

One-Dimensional Photonic Crystal Inner Coated Hollow Fiber Sensor Based on Bloch Surface Wave With Ultra-High Figure of Merit

Volume 13, Number 1, February 2021

Yi-Xiao Tang
Xian Zhang
Xiao-Song Zhu
Yi-Wei Shi

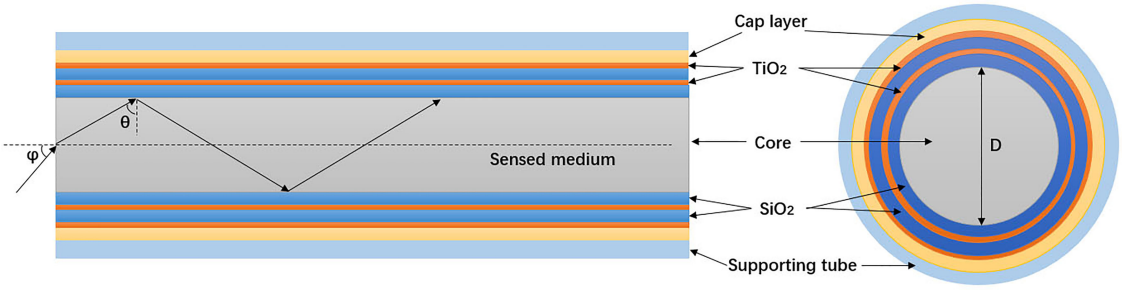

DOI: 10.1109/JPHOT.2020.3044879

One-Dimensional Photonic Crystal Inner Coated Hollow Fiber Sensor Based on Bloch Surface Wave With Ultra-High Figure of Merit

Yi-Xiao Tang,[1] Xian Zhang,[1] Xiao-Song Zhu ,[1,2] and Yi-Wei Shi [1,2]

[1]School of Information Science and Engineering, Fudan University, Shanghai 20433, China
[2]Key Laboratory for Information Science of Electromagnetic Waves (MoE), Fudan University, Shanghai 20433, China

DOI:10.1109/JPHOT.2020.3044879

Manuscript received July 31, 2020; revised November 27, 2020; accepted December 11, 2020. Date of publication December 15, 2020; date of current version December 31, 2020. This work was supported in part by the National Natural Science Foundation of China under Grant 61975034 and in part by the Natural Science Foundation of Shanghai under Grant 19ZR1405000. Corresponding author: Xiao-Song Zhu (e-mail: zhuxiaosong@fudan.edu.cn).

Abstract: A high-performance Bloch surface wave (BSW) sensor based on the hollow fiber (HF) inner coated with the one-dimensional photonic crystal (1DPC) consisting of TiO_2 and SiO_2 bilayers is proposed. Performances including sensitivity and figure of merit (FOM) of the sensor are investigated theoretically with the ray transmission model. Several structure parameters such as the center wavelength of 1DPC, the thickness of the cap layer and the bilayer period are optimized to obtain a best performance of the sensor. The results show that the proposed sensor has an ultra-high FOM over 1100 RIU^{-1}, which is approximately two and one orders of magnitude higher than that of the HF surface plasmon resonance (SPR) sensor and HF long-range SPR sensor, respectively. Moreover, the proposed sensor has a much broader practical RI detection range, which makes it more useful in sensing applications. The performance of the proposed sensor applicated in temperature sensing is also estimated to prove its application potential.

Index Terms: 1DPC, hollow fiber, Bloch surface wave.

1. Introduction

Surface electromagnetic wave is a kind of electromagnetic mode confined at the surface of a medium. The distribution of electromagnetic field decays exponentially away from the interface towards both sides, and the energy is highly concentrated at the interface. A typical kind of surface electromagnetic wave is the surface plasmon polaritons (SPPs) which are usually excited at the interface between metallic and dielectric media. As the high sensitivity of SPPs to the surface properties [1], [2], surface plasmon resonance (SPR) sensors have been widely used for imaging and sensing [3]–[7]. Bloch surface wave (BSW), another kind of surface wave which propagates at the interface between the dielectric media and one-dimensional photonic crystal (1DPC), has attracted much attention in the last decade [8]–[10]. Due to the much lower loss, the resonance dip caused by the excitation of BSW is far narrower than that of SPPs [11], leading to a higher detection accuracy of the sensors. Many kinds of sensors based on the BSW have been studied both theoretically and experimentally in the past decade [12]–[16].

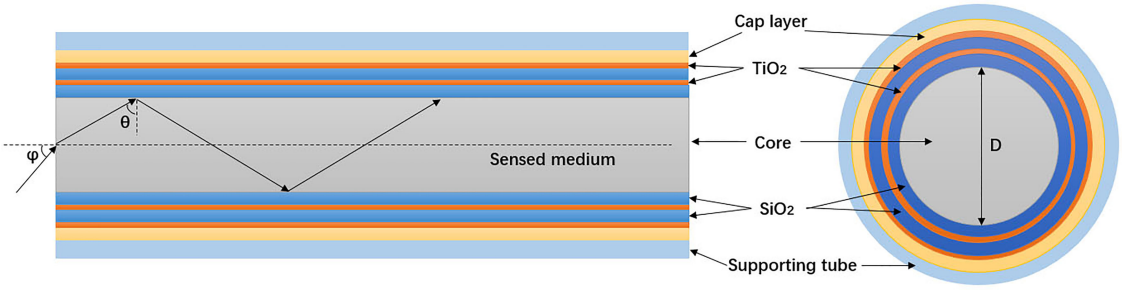

Fig. 1. Schematic and ray transmission model of the designed HF sensor.

Because the excitation of both SPPs and BSW requires phase matching which is usually realized by total reflection condition, most sensors generally adopt the Kretschmann or Otto configurations with a prism [17]. To avoid the bulky disadvantage caused by the prism, many kinds of optical fiber sensors characterized by miniaturization, low cost and high sensitivity were studied in recent years [18], [19]. Among these fibers with various structures, the hollow fiber (HF) which consists of a supporting tube with metallic and dielectric films coated on its inner surface and a hollow core has also been applied for sensing due to its unique advantages [20], [21]. The hollow core is used for transmitting light while containing the sensed liquid medium, saving the space for an external cavity and avoiding the problem for processing the cladding of the fiber. However, most of the studies of the HF sensor is based on SPR [22], [23]. As far as we know, the study of the HF BSW sensor has not been reported.

In this work, we present a high-performance BSW sensor based on the HF inner coated with the 1DPC. The performance of the sensor is analyzed theoretically with the ray transmission model. The structure parameters of the sensor such as the center wavelength of 1DPC, the thickness of the cap layer and the bilayer periods are optimized to achieve the best performance. A comparison is also made between the proposed HF BSW sensor and the HF SPR sensor. The results show that the figure of merit (FOM) of the proposed sensor is two orders of magnitude higher than that of the conventional SPR sensor. The performance of the proposed sensor in temperature sensing is also briefly estimated to indicate its application potential.

2. Sensor Design and Theory

The lengthwise and transverse sections of the designed HF sensor are shown in Fig. 1. The multilayers of the cap layer and the 1DPC are sequentially coated on the inner surface of the hollow core of the silica tube. Similar kinds of multilayer structures have already been successfully fabricated in the HF by the liquid phase deposition method [24]. The atomic layer deposition technique is also a suitable candidate for the coating method to realized higher quality multilayers [25]. The ray transmission model is also illustrated with the transmitted light in the figure. This model has been proved to be very appropriate for the theoretical analysis of the HF sensors by the high consistency between the theoretical and experimental results in previous work [23], [26]. The liquid sensed medium with refractive index (RI) higher than that of the fused silica is filled in the hollow core, so the input light will total reflect on the inner surface of the 1DPC when it transmits in the liquid core. If the wave vector of the input light matches that of the BSW on the interface between the cap layer and the supporting tube, the BSW would be excited. Then a corresponding resonance dip would appear in the transmission spectrum when appropriate broadband light transmits in the core.

We adopt TiO_2 layer and SiO_2 layer to compose the 1DPC structure, with RI $n_1 = 2.36$ [27] and $n_2 = 1.46$, respectively. These two kinds of materials are almost transparent in the visible spectrum and commonly used in the 1DPC applications [14], [16]. The extinction coefficient of the

two materials is set as 10^{-4}. The thickness of the two layers is denoted by d_1 and d_2, which is given by the quarter-wave film system [28] as

$$n_1 d_1 = n_2 d_2 = L_0/4, \tag{1}$$

where L_0 is the center wavelength of the band gap of 1DPC. TiO_2 is adopted as the material of the cap layer which is used to control the property of the sensor.

According to the ray transmission model in Fig. 1, we can theoretically calculate the transmission spectrum of the proposed sensor. Assume that the input light has a standard Gaussian profile with a power distribution expressed as

$$P_{in}(\varphi) \propto \exp(-\varphi^2/\varphi_0(\lambda)^2), \tag{2}$$

where φ is the incident angle of a specific plane wave component, and φ_0 is the divergence angle. The power distribution of output light of the HF BSW sensor is given as

$$P_{out} = \int_{\theta_{\min}}^{\pi/2} P_{in}(\theta) R(\theta)^{N(\theta)} d\theta, \tag{3}$$

where θ_{min} is the minimum incident angle, and θ is the angle between the normal of the reflection interface and the direction of the incident light. $R(\theta)$ represents the reflectance on the inner surface of the HF, which can be calculated by the transfer matrix method [11]. It would be different for the p-polarized and s-polarized light, i.e., the TM and TE light. $N(\theta)$ is the number of reflections of the incident light through the HF which can be calculate by $N(\theta) = L\cot\theta/D$. L and D is the length and diameter of the HF, which is 5cm and 700μm in our calculation, respectively.

Finally, the generalized expression for the transmittance of the HF BSW sensor can be expressed as

$$T = \frac{\int_{\theta_{\min}}^{\pi/2} P_{in}(\theta) R(\theta)^{N(\theta)} d\theta}{\int_{\theta_{\min}}^{\pi/2} P_{in}(\theta) d\theta}. \tag{4}$$

While BSW is excited, part of the energy of the incident light is transferred to the BSW, bringing a severe decrease of reflectivity. It would form a resonance dip in the transmission spectrum at a particular wavelength, known as the resonance wavelength (RW) which changes along with the RI of the sensed medium. Therefore, the RI of the sensed medium could be obtained by measuring the RW from the transmission spectra [29].

Sensitivity of the sensor is determined by the shift in the RW ($\Delta\lambda_{res}$) due to the RI change of sensed medium (Δn_0) as

$$S = \frac{\Delta\lambda_{res}}{\Delta n_0}. \tag{5}$$

How accurately the value of RW can be determined depends on the full width at half maximum (FWHM) of the transmittance curve. The overall performance of a sensor is defined in terms of FOM as

$$FOM = \frac{S}{FWHM}. \tag{6}$$

When the sensor is adopted for temperature sensing, the temperature sensitivity is determined by the shift in the RW due to the temperature change (ΔT) as

$$S_T = \frac{\Delta\lambda_{res}}{\Delta T}. \tag{7}$$

3. Results and Discussions

To investigate the performance of the proposed HF sensor, we firstly calculate the transmission spectrum when the center wavelength of 1DPC is 1000 nm. The RI of the sensed medium n_0, the

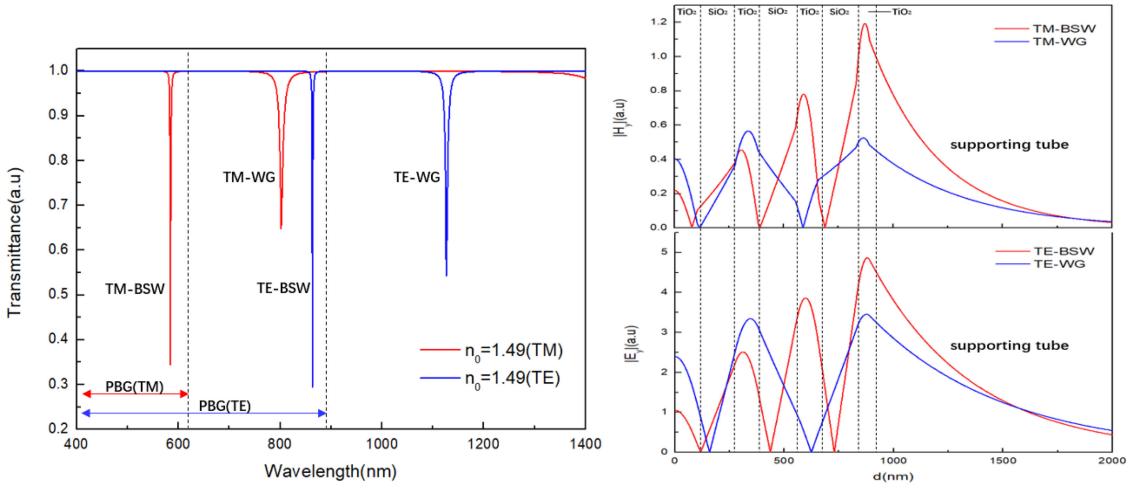

Fig. 2. (a) Transmission spectra of the proposed HF sensor at $n_0 = 1.49$, $N = 3$, $L_0 = 1000$ nm, $d_{cap} = 60$ nm. (b) Electric field distribution at the resonance wavelength 584 nm, 802 nm, 863 nm and 1126 nm.

bilayer periods N and the cap layer thickness d_{cap} are 1.49, 2 and 60 nm, respectively. Figure 2(a) shows the transmission spectra of both p-polarized and s-polarized incident lights, i.e., TM and TE lights, in red and blue solid lines. Figure 2(b) shows the corresponding electric field distributions in the multilayer structure at the resonance dips in the spectra [30]. From Fig 2(a) we can see both TM and TE incident light excite two resonance dips in the wavelength range as shown. For the TM light, the gradually attenuated oscillating electric filed in 1DPC and the enhancement at the cap layer shown in Fig 2(b) indicate that the dip at 584 nm which locates in the photonics bandgap (PBG) is caused by the excitation of the BSW. The dip at 802 nm is caused by the waveguide mode (WG) which could also distinguished by its oscillating electric filed in 1DPC. The situation is similar for the TE light. Distinguished by the electric field distributions of the dips, the dip at 863 nm in the PBG is caused by the BSW and the dip at 1126 nm is caused by the WG. The range of the PBG of 1DPC is also shown in Fig 2(a) and we just consider the situation when the incident light is p-polarized in later analysis.

Unlike the SPR, the BSW could be excited by both TM and TE lights. There are some differences between the sensing properties of these two polarized lights. Figure 3(a) shows the variations of the transmission spectra of both TM and TE lights when the sensed RI changes from 1.49 to 1.50. Both TM and TE BSW resonance dips blue-shift as the sensed RI increases. The variation of the RWs with different sensed RIs and the linear fit results are shown in Fig. 3(b). According to the slopes of the linear fitting results, the average sensitivity of the TM and TE lights are 1718 nm/RIU and 1233 nm/RIU, respectively, which means the TE light has a little bit lower sensitivity than the TM light. Moreover, because the TE PBG is much wider than the TM PBG, the resonance dip of the TM-WG is still in the TE PBG and very close to the TE BSW resonance dip. It will definitely cause interference if the TE BSW resonance dip is used for sensing. On the contrary, the TM BSW dip, which is far from all other resonance dips, is a better choice for sensing than the TE BSW dip in the proposed sensor. Thus, only the performance of the TM BSW resonance in the sensor is investigated hereafter.

In the designed sensor, the input light transmits in the liquid sensed medium filled in the hollow core of the fiber. Because most liquid have absorption band in the near infrared region, 400-800 nm is adopted as the operation spectrum range. Then the PBG of the TM light must locate in this range to guarantee that the TM BSW RW is within 400-800 nm. Figure 4 shows the PBGs of the 1DPC with different center wavelengths. The left half represents TM light and the right half represents TE

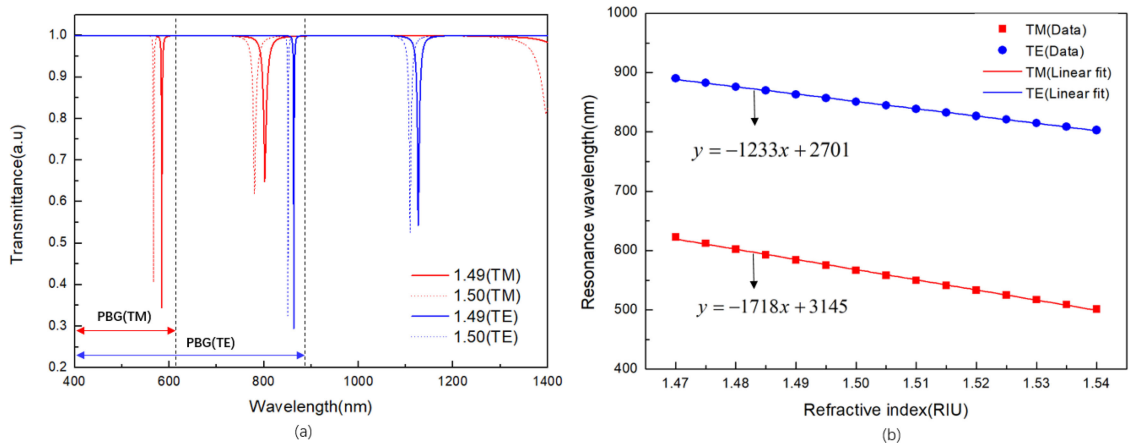

Fig. 3. (a) Transmission spectra of the proposed sensor at varied n_0 with $L_0 = 1000$ nm, $d_{cap} = 60$ nm, $N = 3$. (b) Dependence of RW on RI of the sensed medium for both TM- and TE-polarized light.

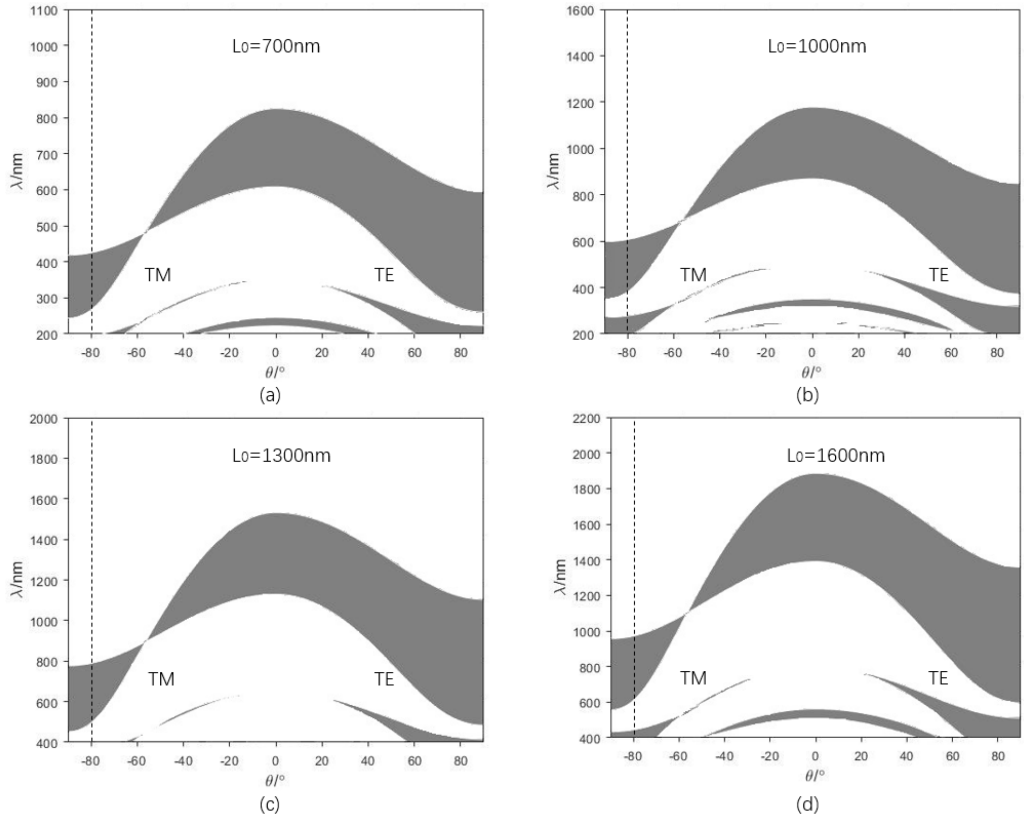

Fig. 4. photonic bandgap of 1DPC with different center wavelength at $n_0 = 1.49$. The left side represents TM-polarized light, while the right side represents TE-polarized light. (a) $L_0 = 700$ nm, (b) $L_0 = 1000$ nm, (c) $L_0 = 1300$ nm, (d) $L_0 = 1600$ nm.

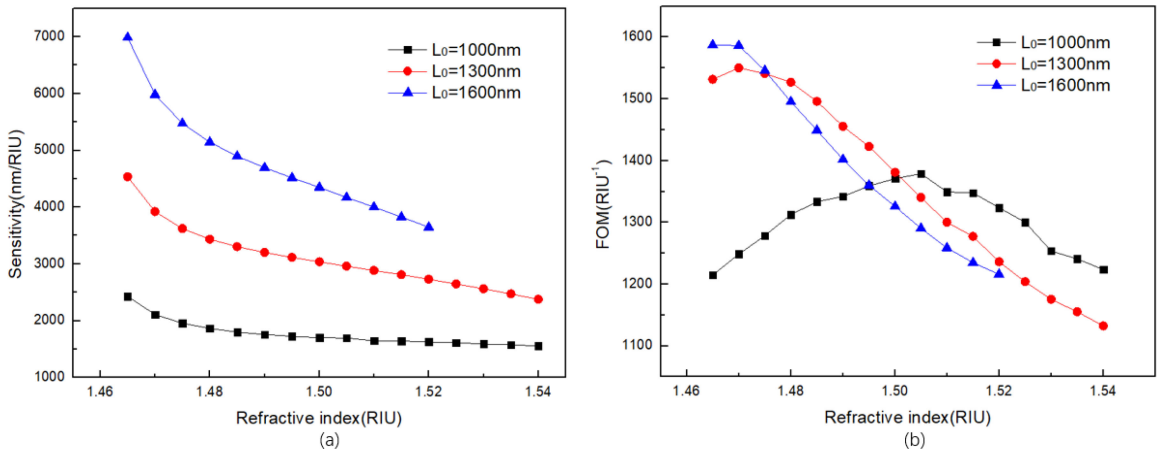

Fig. 5. Theoretical results of the performance for the proposed sensor with different center wavelength. (a) Sensitivity versus n_0. (b) FOM versus n_0.

light. The shaded part represents wavelengths that are forbidden to propagate in the 1DPC, i.e., the PBG. According to the ray transmission model in Fig. 1 and the Gaussian power distribution of the input light, most transmitted lights in the fiber sensor have a large incident angel near 90° on the 1DPC surface, so the PBG of TM light with incident angles larger than 80° should be focused on. The dashed line in Fig. 4 marks the incident angle of 80°. It can be seen that the TM PBG red-shifts as the center wavelength increases. The majority part of the PBG is in the 400-800 nm range while the center wavelength is between 1000 and 1600 nm. In particular, the PBG covers almost all the operation wavelength range when the center wavelength is 1300 nm as shown in Fig. 4(c). On this basis, 1300 nm is an appropriate choice for the center wavelength.

In order to further determine the optimal center wavelength, the sensitivity and FOM of the designed sensor with different center wavelengths are analyzed and shown in Fig. 5. It can be seen from Fig. 5(a) that the sensitivity of the sensor increases with the center wavelength. However, as shown in Fig. 5(b), the average FOM is highest when the center wavelength is 1300 nm. Moreover, the sensor with the 1600 nm center wavelength has a narrower RI detection range. With consideration of the PBG range and the performance of the sensor, 1300 nm is adopted as the center wavelength in later calculation.

Same as many other kinds of BSW sensors, the cap layer is used to manipulate the property of the proposed sensor since it's inconvenient to change the whole structure of the 1DPC. The thickness of the cap layer has a huge impact on the RW and the sensor's performance. Fig. 6(a) shows the transmission spectra of the proposed sensor with different cap layer thicknesses. The resonance dip around 460 nm is excited by the WG which basically stays still with the cap layer thickness changing. The BSW dip gets closer to the WG dip when the thickness of the cap layer decreases, which may cause interference in detection. From Fig. 6(b) and 6(c), thinner cap layer can bring relatively higher sensitivity of the sensor but narrower detecting range because the resonance dip is closer to the edge of PBG. For the proposed sensor, the detecting range is widest and the average FOM is comparatively higher when the cap layer thickness is 60 nm. Therefore, 60 nm is adopted as the optimal thickness of the cap layer.

The bilayer periods of the 1DPC will influence not only the complexity of fabrication, but also the sensor's performance. Figure 7(a) shows the transmission spectra of the proposed sensor with different bilayer periods. It can be discovered that the depth of the BSW dip shrinks significantly with the increase of the period, which is because the 1DPC is thicker and the restriction of the PBG is stronger with more bilayer periods. The variation of the dip depth of the sensor with different bilayer periods is shown in Fig. 7(b). The dip depth with $N \geq 3$ decreased dramatically to even lower

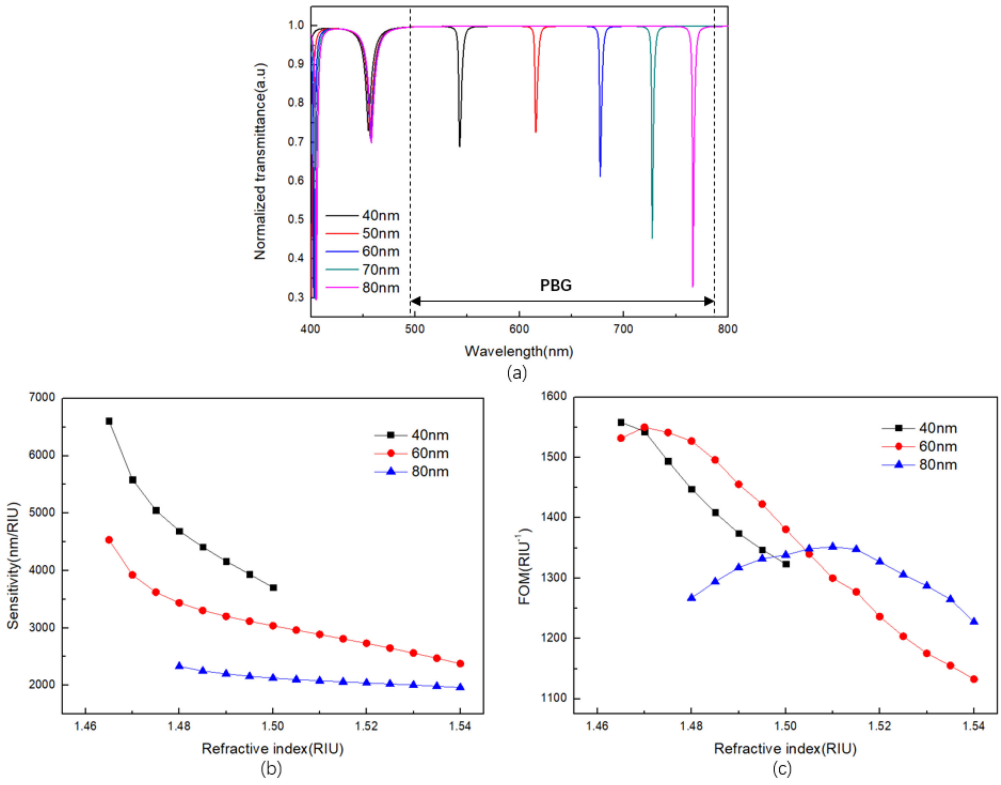

Fig. 6. Transmission spectra and theoretical results of performance for the proposed sensor with different thickness of cap layer. (a) Transmission spectra at $n_0 = 1.49$, $N = 3$ and $L_0 = 1300$ nm. (b) Sensitivity versus n_0. (c) FOM versus n_0.

than 10% which is so shallow that will cause difficulties in distinguishing the RW and reduce the detection accuracy of the sensor. However, for $N = 2$, the dip depth remain larger than 40% in the whole RI range. The Figures 7(c) and 7(d) show the sensitivity and FOM of the proposed sensor, respectively. The sensitivity of the proposed sensor change little with different bilayer periods, while the sensor exhibits better FOM with $N \geq 3$ than $N = 2$ and the difference decreases as RI increases. Regardless the fabrication complexity, $N = 3$ seems to be the optimal choice to achieve best performance. However, it's worth noting that the deviation of the 1DPC structure in fabrication may decrease the performance and the fabrication of similar kind of HF with $N = 2$ has already been proved feasible experimentally [24]. So $N = 2$ is a more reasonable choice for experimental consideration.

An overall comparison of performances is made between the proposed sensor and the HF sensors based on SPR [23] and long-range SPR (LRSPR) [24], as shown in Table 1. Since there is hardly any liquid with RI higher than 1.62, the proposed HF BSW sensor has a much broader practical RI detection range than both HF SPR sensor and HF LRSPR sensor. The HF BSW sensor has comparable sensitivity to the HF SPR sensors. However, owing to the narrow width of the resonance dip, it has an ultra-high FOM approximately two and one orders of magnitude higher than the HF SPR sensor and HF LRSPR sensor, respectively.

In the HF BSW sensor, it is the bulk RI rather than surface RI of the sensed medium which is detected. It may be not very adaptive for the bio-molecular sensing which is mainly based on the RI change of the surface. However, the applications based on sensing the change of bulk RI, such as temperature monitoring, are very suitable for this sensor [31], [32]. It could be easily turned into a high performance temperature sensor by filling with some liquid with high RI and high thermal

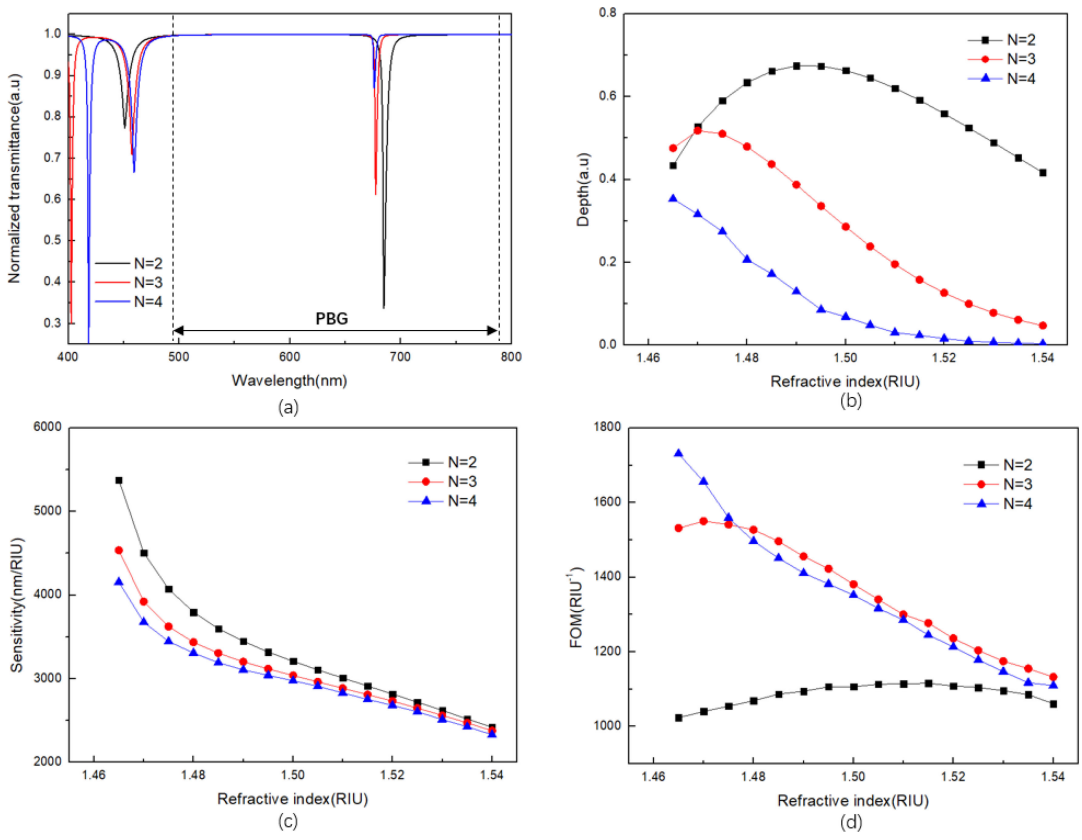

Fig. 7. Transmission spectra and theoretical results of performance for the proposed sensor with different bilayer period. (a) Transmission spectra at $n_0 = 1.49$, $d_{cap} = 60$ nm and $L_0 = 1300$ nm. (b) Depth of resonance dips versus n_0. (c) Sensitivity versus n_0. (d) FOM versus n_0.

TABLE 1
Comparison Between the Proposed Sensor and HF SPR/LRSPR Sensors

Configuration	Detection RI range RIU	Sensitivity nm/RIU	FOM RIU^{-1}
HF BSW sensor with 1DPC (L_0=1300nm, N=3, d_{cap}=60nm)	1.465-1.62	2378-4534	1132-1531
HF SPR sensor	1.509-1.763	2185-6607	12-25
HF LRSPR sensor	1.477-1.50	3657-10961	139.8-152.6

RI coefficient. Take for example the mixed solutions of white oil and polymethylphenyl silicone oil [24], whose RI decreases linearly from 1.519 to 1.501 as the temperature rises from 20 °C to 60 °C according to our measurement. The transmission spectra of the HF BSW sensor filled with this mixed solution at different temperatures are shown in Fig. 8(a). An average temperature sensitivity of 1.376 nm/ °C can be obtained from the slope of the fitting result from Fig. 8(b) for the proposed sensor, which is comparable to the fiber SPR sensors. However, the resolution of such

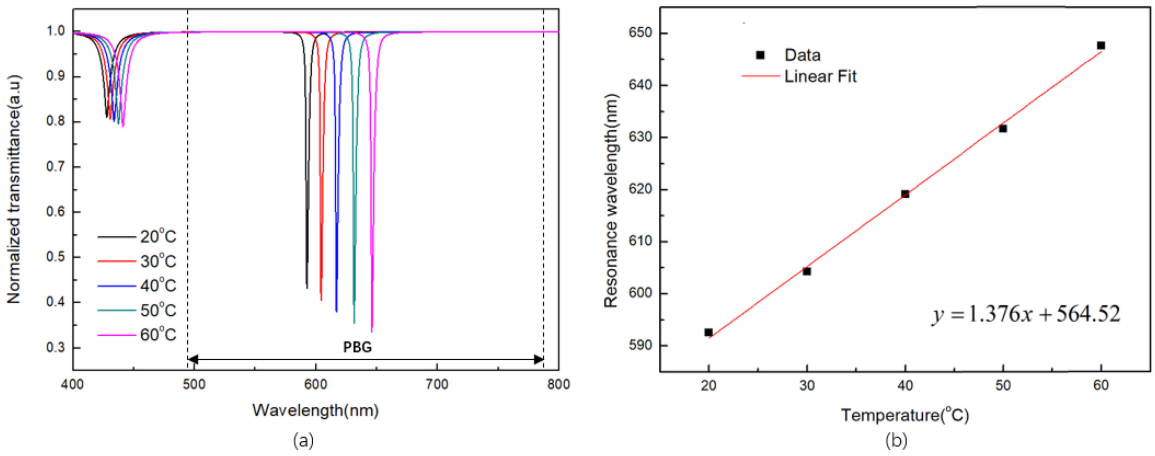

Fig. 8. Transmission spectra and performance of the proposed sensor with white oil/polymethylphenyl silicone oil mixture. $L_0 = 1300$ nm, $d_{cap} = 60$ nm and $N = 2$. (a) Transmission spectra with different temperatures. (b) Linear relationship between the RW of the sensor and temperature.

temperature sensor will be much higher than the SPR based temperature sensors because of its ultra-high FOM.

4. Conclusion

In conclusion, we present a high-performance HF sensor based on the BSW. The 1DPC composed of TiO_2 and SiO_2 bilayers and an additional cap layer are coated on the inner surface of the HF to support and manipulate the excitation of BSW. Performances including sensitivity and FOM of the sensor were evaluated theoretically with a ray transmission model. Several structure parameters such as the center wavelength of 1DPC, the thickness of the cap layer and the bilayer period were optimized to obtain the best performance of the sensor. The results show that the FOM of the proposed sensor reaches more than 1100 RIU^{-1}, which is approximately two and one orders of magnitude higher than that of the HF SPR sensor and the HF LRSPR sensor, respectively. Moreover, the proposed sensor has a much broader practical RI detection range than both HF SPR sensor and HF LRSPR sensor, which make it more useful in sensing applications. An estimation about the performance of the proposed sensor in temperature sensing was also made to prove its application potential. The results of this work could make some contribution to the research of optical fiber BSW sensors.

References

[1] H. Šípová, S. Zhang, A. M. Dudley, D. Galas, K. Wang, and J. Homola, "Surface plasmon resonance biosensor for rapid label-free detection of microribonucleic acid at subfemtomole level," *Anal. Chem.*, vol. 82, no. 24, pp. 10110–10115, 2010.
[2] L. Li, Y. Liang, Q. Liu, and W. Peng, "Dual-channel fiber-optic biosensor for self-compensated refractive index measurement," *IEEE Photon. Technol. Lett.*, vol. 28, no. 19, pp. 2110–2113, Oct. 2016.
[3] R. K. Verma, A. K. Sharma, and B. D. Gupta, "Surface plasmon resonance based tapered fiber optic sensor with different taper profiles," *Opt. Commun.*, vol. 281, no. 6, pp. 1486–1491, 2008.
[4] J. N. Dash, R. Das, and R. Jha, "AZO coated microchannel incorporated PCF-based SPR sensor: A numerical analysis," *IEEE Photon. Technol. Lett.*, vol. 30, no. 11, pp. 1032–1035, Jun. 2018.
[5] C. Liu *et al.*, "Analysis of a surface plasmon resonance probe based on photonic crystal fibers for low refractive index detection," *Plasmonics*, vol. 13, no. 3, pp. 779–784, 2018.
[6] Y. Zhang, F. Tian, Z. Su, R. Bai, and J. Zhang, "Broadband single-polarization optical fiber based on surface plasmon resonance," *Appl. Opt.*, vol. 59, no. 3, pp. 779–784, 2020.

[7] C. Liu *et al.*, "Surface plasmon resonance (SPR) infrared sensor based on D-shape photonic crystal fibers with ITO coatings," *Opt. Commun.*, vol. 464, 2020, Art. no. 125496.
[8] R. D. Meade, K. D. Brommer, A. M. Rappe, and J. D. Joannopoulos, "Electromagnetic bloch waves at the surface of a photonic crystal," *Phys. Rev. B*, vol. 44, no. 19, pp. 10961–10964, 1991.
[9] Y. C. Hsu and L. W. Chen, "Bloch surface wave excitation based on coupling from photonic crystal waveguide," *J. Opt.*, vol. 12, no. 9, 2010, Art. no. 095709.
[10] M. Ballarini *et al.*, "Bloch surface waves-controlled emission of organic dyes grafted on a one-dimensional photonic crystal," *Appl. Phys. Lett.*, vol. 99, no. 4, 2011, Art. no. 043302.
[11] X.-J. Tan and X.-S. Zhu, "Optical fiber sensor based on bloch surface wave in photonic crystals," *Opt. Exp.*, vol. 24, no. 14, pp. 16016–16026, 2016.
[12] M. Gryga, D. Vala, P. Kolejak, L. Gembalova, D. Ciprian, and P. Hlubina, "One-dimensional photonic crystal for bloch surface waves and radiation modes-based sensing," *Opt. Mater. Exp.*, vol. 9, no. 10, pp. 4009–4022, 2019.
[13] T. Y. Tu *et al.*, "Excitation of bloch surface wave on tapered fiber coated with one-dimensional photonic crystal for refractive index sensing," *Opt. Exp.*, vol. 25, no. 8, pp. 9019–9027, 2017.
[14] M. Scaravilli *et al.*, "Excitation of bloch surface waves on an optical fiber tip," *Adv. Opt. Mater.*, vol. 6, no. 19, 2018, Art. no. 1800477.
[15] S. Li, J. Liu, Z. Zheng, Y. Wan, W. Kong, and Y. Sun, "Highly sensitive, bloch surface wave D-Type fiber sensor," *IEEE Sens. J.*, vol. 16, no. 5, pp. 1200–1204, Mar. 2016.
[16] E. Gonzalez-Valencia, R. A. Herrera, and P. Torres, "Bloch surface wave resonance in photonic crystal fibers: Towards ultra-wide range refractive index sensors," *Opt. Exp.*, vol. 27, no. 6, pp. 8236–8245, 2019.
[17] P. K. Maharana, R. Jha, and P. Padhy, "On the electric field enhancement and performance of SPR gas sensor based on graphene for visible and near infrared," *Sensors Actuators B: Chem.*, vol. 207, no. Part A, pp. 117–122, 2015.
[18] J. Homola, "Optical fiber sensor based on surface plasmon excitation," *Sensors Actuators B: Chem.*, vol. 29, no. 1–3, pp. 401–405, 1995.
[19] A. K. Sharma, R. Jha, and B. D. Gupta, "Fiber-optic sensors based on surface plasmon resonance: A comprehensive review," *IEEE Sensors J.*, vol. 7, no. 8, pp. 1118–1129, Aug. 2007.
[20] C. B. Jing *et al.*, "Metallic attenuated total reflection infrared hollow fibers for robust optical transmission systems," *Appl. Phys. Lett.*, vol. 105, no. 1, 2014, Art. no. 011102.
[21] R. George and J. A. Harrington, "Infrared transmissive, hollow plastic waveguides with inner Ag-AgI coatings," *Appl. Opt.*, vol. 44, no. 30, pp. 6449–6455, 2005.
[22] N. Luan and J. Yao, "High refractive index surface plasmon resonance sensor based on a silver wire filled hollow fiber," *IEEE Photon. J.*, vol. 8, no. 1, Feb. 2016, Art. no. 4800709.
[23] B. H. Liu, Y. X. Jiang, X. S. Zhu, X. L. Tang, and Y. W. Shi, "Hollow fiber surface plasmon resonance sensor for the detection of liquid with high refractive index," *Opt. Exp.*, vol. 21, no. 26, pp. 32349–32351, 2019.
[24] X. Zhao, X. Zhang, X.-S. Zhu, and Y.-W. Shi, "Long-range surface plasmon resonance sensor based on the GK570/Ag coated hollow fiber with an asymmetric layer structure," *Opt. Exp.*, vol. 27, no. 7, pp. 9550–9560, 2019.
[25] T. Nam, S. Seo, and H. Kim, "Atomic layer deposition of a uniform thin film on two-dimensional transition metal dichalcogenides," *J. Vac. Sci. Technol. A*, vol. 38, no. 3, 2020, Art. no. 030803.
[26] Y. Matsuura, A. Hongo, M. Saito, and M. Miyagi, "Loss characteristics of circular hollow waveguides for incoherent infrared light," *J. Opt. Soc. Am. A*, vol. 6, no. 3, pp. 423–427, 1989.
[27] M. Utkal and K. Ibrahim, "Smith predictor with sliding mode control for processes with large dead times," *J. Elect. Eng.*, vol. 68, no. 6, pp. 463–469, 2017.
[28] H. A. Macleod, *Thin-Film Optical Filters.* Boca Raton, FL, USA: CRC Press, 2010.
[29] K. Lin, Y. Lu, J. Chen, R. Zheng, P. Wang, and H. Ming, "Surface plasmon resonance hydrogen sensor based on metallic grating with high sensitivity," *Opt. Exp.*, vol. 16, no. 23, pp. 18599–18604, 2008.
[30] A. Shalabney and I. Abdulhalim, "Electromagnetic fields distribution in multilayer thin film structures and the origin of sensitivity enhancement in surface plasmon resonance sensors," *Sensors Actuators A: Phys.*, vol. 159, no. 1, pp. 24–32, 2010.
[31] X. Yang, L. Zhu, M. Dong, and J. Yao, "Multiplex localized surface plasmon resonance temperature sensor based on grapefruit fiber filled with a silver nanoshell and liquid," *Opt. Eng.*, vol. 58, no. 11, 2019, Art. no. 117104.
[32] A. K. Sharma, H. S. Pattanaik, and G. J. Mohr, "On the temperature sensing capability of a fibre optic SPR mechanism based on bimetallic alloy nanoparticles," *J. Phys. D. Appl. Phys.*, vol. 42, no. 4, 2009, Art. no. 045104.